The first stages of oxidation of a-Si: a study of the Si $L_{2,3}$ VV Auger lineshape

1989 J. Phys.: Condens. Matter 1 5783

(http://iopscience.iop.org/0953-8984/1/33/023)

J. Phys.: Condens. Matter 1 (1989) 5783–5792. Printed in the UK

The first stages of oxidation of a-Si: a study of the Si $L_{2,3}VV$ Auger lineshape

R Vidal and M C G Passeggi
Instituto de Desarrollo Tecnológico para la Industria Química, Güemes 3450, 3000 Santa Fe, Argentina

Received 7 October 1988, in final form 10 January 1989

Abstract. We report an independent-electron model calculation of the $L_{2,3}VV$ Auger lineshape for the ideal Si(100) surface with oxygen impurities incorporated at different positions with respect to the surface. The $L_{2,3}VV$ Auger lineshape is compared with experimental spectra measured during the first stages of oxidation of a-Si. The Auger lineshape obtained for an oxygen monolayer over the Si(100) surface in a bridging configuration compares well with experimental spectra.

1. Introduction

The first stages of oxidation of silicon have been extensively studied in the last few years. Different experimental techniques have been employed in order to elucidate the nature of the SiO_2–Si interface. Among others, photo-emision spectroscopy [1–6], electron energy loss spectroscopy [5] and Auger electron spectroscopy (AES) [6–10] have played a major role. As ultraviolet photo-electron spectroscopy (UPS) and AES are essentially valence band spectroscopic techniques, a variation in the shape of the valence band spectra should be associated with a change in the density of electronic states in the solid. This in turn may show features which allow us to infer characteristics of local order effects such as bond lengths, bond angles, coordination numbers and nature of first neighbours [1].

In UPS the valence band spectra are directly comparable with theoretical densities of states weighted by the atomic photo-ionisation cross sections. This makes the comparison between theoretical models and experimental results easy [1, 4, 11]. In AES the core–valence–valence (CVV) spectra cannot be compared directly with the density of electronic states. To obtain a valence band spectra from the CVV Auger lineshape, self-deconvolution of the experimental data is needed [12]. In this form the information obtained by self-deconvolution of $L_{2,3}VV$ Auger spectra of the clean and oxygen-chemisorbed (in the initial oxidation stages) Si(111) 7×7 surface was correlated in [9] with theoretical models. Another form is to compare the experimental Auger CVV lineshape with the self-convoluted theoretical density of states. In this way Si $L_{2,3}VV$ Auger spectra from the (111) surface were compared in [8] with the theoretical density of states. However, the measured valence band Auger lineshapes rarely agree with the predictions of the corresponding density-of-states models. In some cases the agreement is only qualitative as above. For the Si $L_{2,3}VV$ lines, good agreement with the measured

0953-8984/89/335783 + 10 $02.50

Auger lineshapes can be obtained only if the transition matrix element variations across the valence band are taken into account [13].

The energy band structure for the oxygen chemisorbed on the Si(100) surface and for the SiO_2–Si interface were calculated in [14]. The Si $L_{2,3}VV$ Auger transition lineshape was calculated with these results. However, the calculation is not consistent in the sense that relevant Auger matrix elements were obtained empirically for the $L_{2,3}VV$ lines in bulk silicon by a set of parameters selected to fit the experimental results [15].

In a previous work [16] we have calculated the $L_{2,3}VV$ Auger lineshape for the Si(100) surface. We used the extended Hückel approximation for a cluster of silicon atoms to evaluate the valence band states. It was found that reasonable agreement with experimental results can be obtained if Auger matrix elements and free-surface effects are taken into account.

In the present work, we apply the previous model to examine silicon clusters which include the presence of oxygen impurities incorporated at different positions with respect to the (100) surface. The Si $L_{2,3}VV$ Auger lineshapes obtained through this model are compared with experimental spectra measured during the first stages of oxidation of a-Si [10]. The intention is to find out whether one can correlate the theoretical predictions with some preferential configuration of oxygen impurities which occur in the first oxidation stages by comparison with the observed spectra.

To explore which configurations of oxygen on the a-Si surface are more likely to occur from an energy point of view requires a theoretical model able to provide a good estimation of total energies, which is beyond the scope of the extended Hückel method. We have considered here configurations whose stability has been examined through the use of other methods [17, 18] to see how the $L_{2,3}VV$ Auger lineshapes calculated with these configurations may resemble the experimental lineshapes.

2. Theory

The calculation of the Si $L_{2,3}VV$ Auger lineshape have been described in detail in a previous paper [16]; so here we give only a brief description of it, stressing the modifications introduced to take into account the oxygen impurities.

The Auger lineshape could be obtained integrating the differential probability $dw_k/(dE_k\, d\Omega_k)$ for an Auger transition on the exit angle of the Auger electron and averaging over the orientation of the orbital angular momentum of the initial core hole:

$$N(E_k) = \left\langle \int d\Omega_k \frac{dw_k}{dE_k\, d\Omega_k} \right\rangle_{m_\gamma} \tag{1}$$

where

$$\frac{dw_k}{dE_k\, d\Omega_k} = \frac{2\pi}{\hbar} k^2 \frac{dk}{dE_k} \sum_{\mu,\nu}^{oc} [|(\mu\nu|c\boldsymbol{k})|^2 + |(\nu\mu|c\boldsymbol{k})|^2 - \tfrac{1}{2}[(\mu\nu|c\boldsymbol{k})(\nu\mu|c\boldsymbol{k})^* + \text{cc}]\delta(E_k + E_c - E_\mu - E_\nu) \tag{2}$$

$$(\mu\nu|c\boldsymbol{k}) = \int\int d\boldsymbol{r}_1\, d\boldsymbol{r}_2\, \Phi_\mu^*(\boldsymbol{r}_1)\, \Phi_\nu^*(\boldsymbol{r}_2) \frac{e^2}{|\boldsymbol{r}_1 - \boldsymbol{r}_2|} \Phi_c(\boldsymbol{r}_1)\Phi_k(\boldsymbol{r}_2) \tag{3}$$

and $E_k = \hbar^2k^2/2m$ is the kinetic energy of the Auger electron at the electron detector, E_μ and E_ν are the electron energies of the orbitals at the valence band, E_c is the ionisation potential of the core hole orbital, Φ_μ and Φ_ν are the spatial components of the valence

band orbitals, Φ_c is the core hole orbital and Φ_k is the continuum orbital. The sum in equation (2) extends over the whole set of the occupied valence band orbitals.

In order to evaluate the matrix elements $(\mu\nu|c\boldsymbol{k})$, one must specify the form of the valence band orbitals. In the extended Hückel approximation, used here, they are written as a linear combination of atomic orbitals (LCAO) of the following form:

$$\Phi_\mu = \sum_{\alpha i} C^\mu_{\alpha i}\chi_{\alpha i} \tag{4}$$

where $\chi_{\alpha i}$ refers to the αth basis function on atomic site i at position $\boldsymbol{R}_i$. In our case we consider $\chi_{\alpha i}$ as an atomic orbital. The matrix element $(\mu\nu|c\boldsymbol{k})$ can now be written in terms of atomic matrix elements of the form

$$(\mu\nu|c\boldsymbol{k}) = \sum_{\substack{\alpha\beta\\ ij}} C^{\mu *}_{\alpha i}\, C^{\nu *}_{\beta j}\, M_{\alpha i\beta jck} \tag{5}$$

$$M_{\alpha i\beta jck} = e^2 \int\int \mathrm{d}\boldsymbol{r}_1\, \mathrm{d}\boldsymbol{r}_2\, \chi^*_{\alpha i}(\boldsymbol{r}_1)\chi^*_{\beta j}(\boldsymbol{r}_2)\frac{1}{|\boldsymbol{r}_1 - \boldsymbol{r}_2|}\chi_{\gamma l}(\boldsymbol{r}_1)\chi_k(\boldsymbol{r}_2) \tag{6}$$

where $\chi_{\gamma l}$ is the atomic orbital centre on site l which represents the core hole state.

Following the results in [19], to a first approximation, we can restrict the sum in equation (5) to the site where the core hole is present. This means that only intra-atomic matrix elements are retained.

2.1. The extended Hückel method

Within the LCAO method for the non-orthogonal basis set the eigenvalues and eigenstates are found by solving

$$\sum_{\alpha i}(H_{\beta j\alpha i} - ES_{\beta j\alpha i})C_{\alpha i} = 0 \tag{7}$$

where

$$H_{\beta j\alpha i} = \langle\chi_{\beta j}|\mathcal{H}\,|\chi_{\alpha i}|\rangle \qquad S_{\beta j\alpha i} = \langle\chi_{\beta j}|\chi_{\alpha i}\rangle.$$

The sum in equation (7) extends over a finite number of sites and states because we replace the infinite crystal by a cluster of atoms.

In the extended Hückel approximation the Hamiltonian matrix elements are proportional to the overlaps $S_{\beta j\alpha i}$ in accordance with the Wolfsberg and Helmholz or the Ballhausen and Gray [20] proposals. In the latter case this reads

$$H_{\beta j\alpha i} = -K(I_{\beta j}I_{\alpha i})^{1/2}S_{\beta j\alpha i} \tag{8}$$

where K is a constant and $I_{\alpha i}$ is the ionisation potential of the αth orbital centre on site i.

In our case the overlaps were calculated using the valence orbitals of the silicon atom (3s and 3p) and the valence orbitals of the oxygen atom (2s and 2p). The functional form of the radial part of these orbitals is that of the Slater-type functions:

$$\begin{aligned} R_{n_\alpha 1_\alpha}(r) &= N_\alpha r^{n_\alpha - 1}\exp(-\xi_\alpha r)\\ N_\alpha &= [(2n_\alpha)!]^{-1/2}(2\xi_\alpha)^{n_\alpha + 1/2}. \end{aligned} \tag{9}$$

We used for $I_{\alpha i}$, ξ_α and K the values used in [21] for the calculation of the electronic structure of transition metal silicides. For oxygen orbitals the values in [22, 23] were used. Table 1 contains the parameters used in our calculation.

Table 1. Parameters used in the extended Hückel calculation.

	Silicon		Oxygen	
	3s	3p	2s	2p
ξ (au^{-1})	2.25	1.65	2.25	2.23
I (eV)	−14.82	−7.75	−33.84	−17.19
K	2.5		2.5	

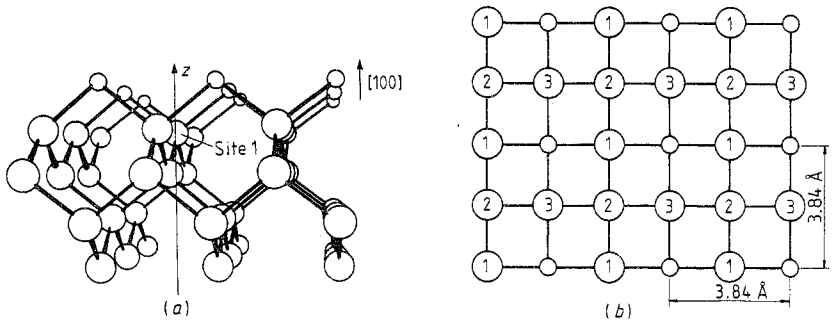

Figure 1. (*a*) A perspective view of a fragment of the silicon cluster used in our model. Small circles represent oxygen atoms adsorbed on the Si(100) surface. (*b*) View of the cluster along the [100] direction. The numbers within the circles represent the atomic layer to which the silicon atom belongs.

The cluster utilised is a hemisphere of 40 silicon atoms. Its planar face coincides with a (100) surface. Oxygen atoms can be in three different configurations.

(i) First they can be substitutional oxygen atoms on the (100) surface.

(ii) Next, substitutional oxygen atom are possible below the (100) surface.

(iii) Finally we have a monolayer of oxygen atoms over the (100) surface. In figure 1, we show a fragment of the cluster where we can appreciate the position of the oxygen atoms over the (100) surface. The distance between the oxygen layer and the first silicon layer was changed from $R_\perp = 1.3575$ Å to $R_\perp = 0.96$ Å. These separations correspond to that in pure silicon and that obtained in [17] for adsorption of oxygen on the Si(100) surface, respectively. In [17] it was found, through a slab simulation within the framework of the SCF pseudopotential approach, that the bridge site configuration is the most stable. This is the configuration shown in figure 1. Very recently it was found [18], by a computer simulation of the thermal oxidation of the Si(100) surface, that the bridging position is energetically the most favoured position of an oxygen adatom on the Si(100) surface. Nevertheless, although in [17] the equilibrium Si–O bond length was found to be 2.15 Å, in [18] the equilibrium Si–O bond length was found to be 1.60 Å which is almost the same as that in bulk SiO_2. According to the model in [18] the Si(100) surface suffers a reconstruction. On the contrary in the model in [17], as in our model, reconstruction of the Si(100) surface is not taken into account.

In order to eliminate the spurious states generated by the dangling bonds of the cluster's boundaries of the undesired surfaces we suppress these states from the matrix $\mathcal{H}$ [24], solving afterwards for the eigenvalues and eigenstates in equation (7). An alternative procedure to terminate the cluster could be performed by saturating the

Table 2. Radial matrix elements for Si $L_{2,3}VV$ Auger decays. We include the results in [27]. In the first and second columns, we indicate the initial valence states of electrons 1 and 2, respectively. The final state of electron 1 is the core hole (2p) while electron 2 is in a continuum orbital with angular momentum l_f. L is the order of the multipolar term in the expansion of the $1/|r_1 - r_2|$ operator. We assume an Auger energy of 95 eV.

		l_f	L	This work	[27]
3s	3s	1	1	1.020×10^{-2}	0.625×10^{-2}
3s	3p	0	1	-0.088×10^{-2}	0.613×10^{-2}
3s	3p	2	1	0.338×10^{-2}	-0.038×10^{-2}
3p	3s	0	0	-0.355×10^{-2}	0.770×10^{-2}
3p	3s	2	2	0.315×10^{-2}	-0.151×10^{-2}
3p	3p	1	0	0.757×10^{-2}	0.788×10^{-2}
3p	3p	1	2	0.328×10^{-2}	0.457×10^{-2}
3p	3p	3	2	0.009×10^{-2}	0.948×10^{-2}

dangling bonds with hydrogen atoms [25]. This will cause the spurious orbitals due to the dangling bonds, which usually appear on top of the valence band, to go down well inside the valence band and they might be counted in the calculation of the Auger process. Although no unique solution can be offered in this sense, one may think that, as long as the cluster size is kept sufficiently large, this procedure should produce similar results, taking into account the localised nature of the Auger process.

The electron energies of the valence band orbitals, which enter into the evaluation of the Auger electron kinetic energy in equation (2), were calculated from the eigenvalues in equation (7). These eigenvalues were shifted in such a way that the energy of the orbital at the top of the valence band coincides with minus the work function of the Si(100) face ($\varphi = 4.8$ eV). In this way the Hückel approximation provides us with a set of relative valence band orbital energies.

2.2. Calculation of the matrix elements

The calculation of these elements has been detailed in [13, 16]. We selected for the radial part of the bonded states a linear combination of Slater-type functions:

$$f(r) = \sum_{\lambda} C_{n\lambda}[(2n_\lambda)!]^{-1/2}(2\xi_\lambda)^{n_\lambda+1/2}r^{n_\lambda-1}\exp(-\xi_\lambda r) \tag{10}$$

where the $C_{n\lambda}$ and the ξ_λ coefficients were calculated in [22]. The continuum electron wavefunction was taken as a Coulombian wavefunction [26].

In table 2, we show some numerical results corresponding to the radial matrix elements. We also include in this table the results in [27]. We believe that the poor agreement between the results in [27] and ours could be ascribed to differences in the continuum wavefunctions used. In [27] a continuum wavefunction generated as a numerical solution to the Coulomb wave equation for the potential of a Herman–Skillman ion with the appropriate core hole is employed. We use a Coulombic wavefunction with an effective charge $Z = 4$. This value was chosen empirically to fit the experimental silicon Auger lineshape.

3. Results

The Auger lineshape of the Si $L_{2,3}VV$ transition for the different configurations of oxygen atoms on the Si(100) surface were obtained by adding the Auger signals cor-

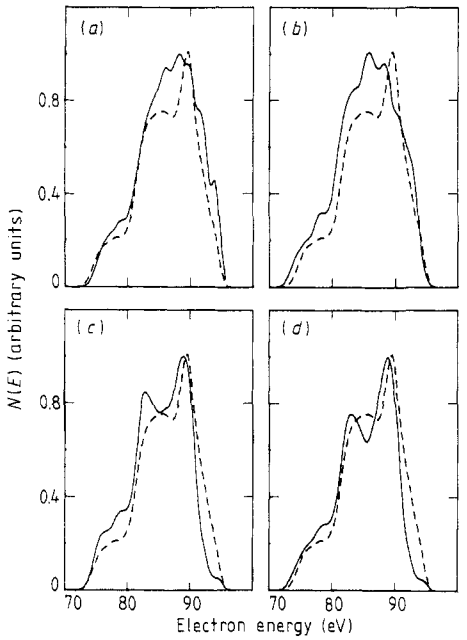

Figure 2. Theoretical Si $L_{2,3}VV$ Auger lineshapes for the silicon cluster with oxygen impurities: (*a*) a substitutional oxygen atom on the (100) surface; (*b*) a substitutional oxygen atom below the (100) surface; (*c*) a monolayer of oxygen atoms ($R_\perp$ = 1.3575 Å); (*d*) as (*c*) but with $R_\perp$ = 0.96 Å. The $L_{2,3}VV$ Auger signals of the ideal Si(100) surface [15] (– – –) are also shown.

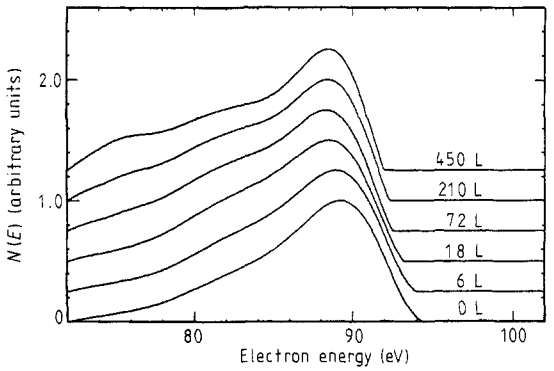

Figure 3. Experimental Si $L_{2,3}VV$ Auger spectra [10]. Values of the oxygen exposure (1 L = 10^{-6} Torr s) are indicated for each spectrum.

responding to different atomic layers weighted with the factor $\exp(-x/\lambda)$, where x is the perpendicular distance of the layer to the (100) surface and λ is the mean escape depth of Auger electrons (a value of λ = 5.2 Å [16] was used for the Si $L_{2,3}VV$ line). This factor takes into account the inelastic energy loss of the Auger electron on its way towards the surface. The Auger signal of one layer is obtained by adding the Auger signals of the different silicon atoms inside a cylinder of radius R and whose axis coincides with the z axis of the cluster (see figure 1). Auger transitions provided by atoms near the boundaries (other than the (100) surface) were not included to avoid spurious effects due precisely to their proximity to these boundaries.

The Auger lineshapes are shown in figure 2. In this figure we also include the Auger lineshape of the Si $L_{2,3}VV$ transition corresponding to the ideal Si(100) surface [16].

In figure 3 we show the Auger spectra obtained during the first stages of oxidation of a-Si [10]. The first-derivative spectra shown in [10] were integrated and subjected to a background subtraction following the procedure in [28].

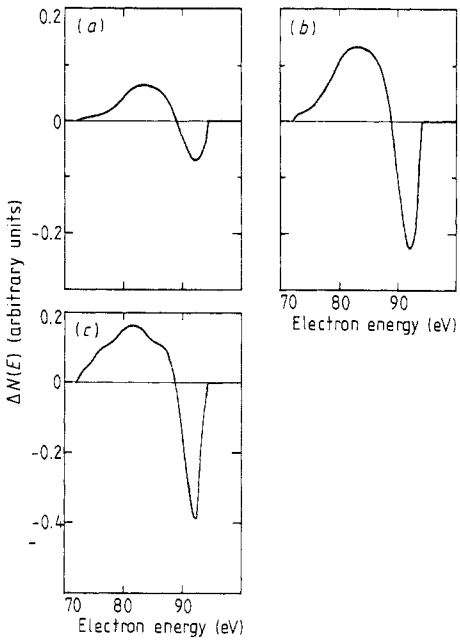

Figure 4. Experimental difference spectra obtained by subtracting the normalised spectra corresponding to different oxygen exposures from the spectrum of pure a-Si: (*a*) 6 L; (*b*) 18 L; (*c*) 72 L.

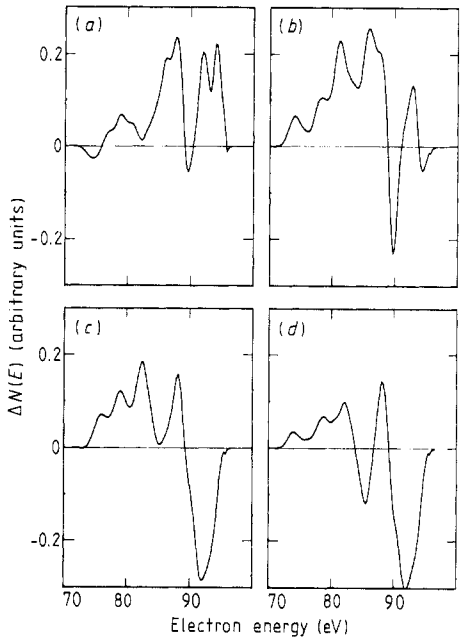

Figure 5. Theoretical difference spectra obtained by subtracting the normalised spectra corresponding to different oxygen arrangements from the spectrum of the ideal Si(100) surface: (*a*) superficial oxygen; (*b*) subsuperficial oxygen; (*c*) a monolayer of oxygen atoms ($R_{\perp}$ = 1.3575 Å); (*d*) same as (*c*) but with $R_{\_}$ = 0.96 Å.

To facilitate the comparison between experimental and theoretical spectra and to make evident the changes introduced by the oxygen incorporation, we subtract the normalised spectra corresponding to different oxygen exposures from the spectrum of pure a-Si (see figure 4). In the same form we subtract from the theoretical spectra shown in figure 2 the theoretical spectrum obtained for the ideal Si(100) surface. These difference spectra are shown in figure 5.

4. Discussion

From the experimental difference spectra shown in figure 4, we can see that the Auger signal shows a reduction on the high-energy side as the oxygen exposure proceeds. This is related to a decrease in the dangling bond states (or in a more general form in the weakly bound states) near the top of the valence band when oxygen is incorporated in the Si(100) surface.

The Auger theoretical difference signal corresponding to a monolayer of oxygen without relaxation (R = 1.3575 Å) resembles the experimental spectra. When the bulk density ρ of 2.2 g cm^{-3} [5] of silicon, the mean escape depth λ of the Auger electron of 6.5 Å [10] and the relation between the thickness of the SiO_x layer and the oxygen exposure are taken into account [10], we can estimate that about 5 L are needed to form a monolayer of oxygen. The assumption made in comparing experimental results obtained for the a-Si surface exposed to oxygen with theoretical results of oxygen

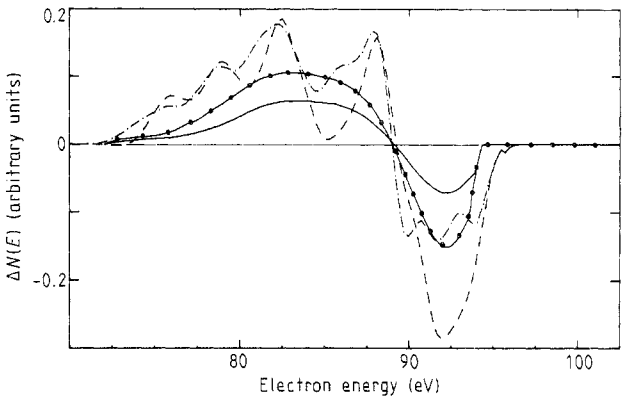

Figure 6. A theoretical difference spectrum corresponding to an oxygen monolayer on the Si(100) surface (– – –), a theoretical difference spectrum obtained by the combination of 60% of the oxygen monolayer spectrum with 40% of the oxygen subsuperficial spectrum (— · —), an experimental difference spectrum corresponding to an a-Si surface exposed to 12 L oxygen (—●—) and an experimental difference spectrum corresponding to an a-Si surface exposed to 6 L oxygen (——).

impurities on the c-Si(100) surface is that the disorder effect is simulated in our model by considering not a unique configuration for the atomic adsorption but a superposition of several configurations. In figure 6, we compare the difference spectra of the a-Si surfaces exposed to 6 and 12 L oxygen, the theoretical difference spectrum corresponding to an oxygen monolayer on the Si(100) surface and the theoretical difference spectrum obtained by the combination of the oxygen monolayer spectrum with the oxygen subsurface spectrum. In the oxygen subsurface spectrum the oxygen concentration is equivalent to 0.17 monolayer. From this figure, we observe that the theoretical spectra resemble the experimental spectra in a qualitative manner. This suggests that oxygen atoms may form, preferentially, a monolayer over the a-Si surface, although the presence of oxygen atoms below the surface cannot be discarded. This is not surprising since the experimental spectra correspond to an a-Si surface and not to a c-Si surface. On the a-Si surface, the oxygen atoms are probably not in a unique arrangement and the experimental Auger signal obtained from this surface may represent an average over various oxygen configurations.

It could be of interest to evaluate the influence on the Auger Si $L_{2,3}VV$ lineshape of the inter-to-intra-atomic Auger transitions. Following the approximation in [19], we can estimate the order of magnitude of the different transitions. For the Si LVV Auger intra-atomic transition the transition rate is about 5×10^{-4} au. On the contrary, for an intra-to-inter-atomic Auger transition (of the type $Si_{2p} \rightarrow Si_{3s}O_{2p}$ or $Si_{2p} \rightarrow Si_{3p}O_{2p}$) the transition rate is about 1×10^{-5} au if a Si–O bond length of 1.6 Å is considered. Thus we conclude that the inter-atomic Auger transition rate is well below that of the intra-atomic Auger rate (about 50 times). In this way, inter-atomic Auger transitions would not have a great influence on the Si $L_{2,3}VV$ Auger transition lineshape.

As pointed out in [29], it is clear that, except in highly ionic materials, only the atomic charge contributes to the Auger current and that the Auger lineshape is sensitive to variations in the local atomic charge density across the valence band. To correlate this local atomic charge density with the $L_{2,3}VV$ Auger signal, we calculated the charge difference in site 1 of the cluster (see figure 1) between the situation where an oxygen atom is located in the place of a silicon atom. To calculate the atomic charge density, we

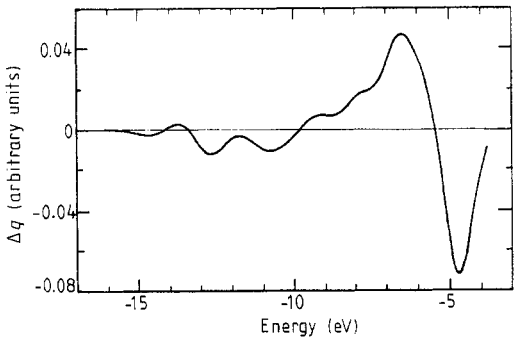

Figure 7. Charge difference in site 1 of the cluster between the situation where an oxygen atom is located in the place of a silicon atom. The energies refer to the vacuum level.

follow the population analysis in [30]. The result is shown in figure 7, where energies refer to the vacuum level. To compare this charge density with the theoretical Auger lineshape differences shown in figure 5(*a*), we must take into account the Auger electron kinetic energy:

$$E_k = E_c - E_\mu - E_\nu. \tag{11}$$

At about 94 eV the Auger signal increases. This can be correlated with a charge transfer of the oxygen atom to the silicon array (a negative charge difference) at energies of the order of 5 eV. At 90 eV the Auger signal decreases and this correlates with a charge transfer of the silicon atoms to the oxygen atom (positive charge difference) at about 7 eV. Between about −13 and −9 eV there is a charge transfer from the oxygen atom to the silicon atoms and this is related to an increase in the Auger signal in the range 78–84 eV. We recall here that this comparison is only qualitative as the charge-density estimation is only approximated since charge self-consistency has not been included. Furthermore, in the present analysis, matrix element effects are ignored; this may cause large charge transfers to produce a minimal effect on the Auger signal.

In our simplified model, we do not take into account the effects of screening in the initial state and final state hole–hole correlation effects. These effects have been discussed well in [31]. We estimate that to a first-order approximation these effects can be disregarded. This approximation is suggested because, for the Si(100) surface, fairly good agreement is found between the theoretical and experimental Si $L_{2,3}VV$ Auger lineshapes without considering screening or/and correlation effects [16].

5. Conclusions

We have presented a model for the calculation of the Si $L_{2,3}VV$ Auger lineshape for a cluster of silicon atoms with oxygen atoms in it. The calculation is consistent in the sense that valence band electronic states and Auger matrix elements are calculated from a similar atomic basis set. The Auger lineshape obtained for an oxygen monolayer over the Si(100) surface in a bridging configuration compares well with experimental spectra. However, the oxygen subsurface contribution cannot be disregarded. Also Auger lineshape variations can be correlated with charge transfer effects between oxygen and silicon atoms. We have estimated that inter-atomic Auger transitions do not play a major role in the determination of the Si LVV Auger lineshape.

Finally it should be emphasised that our model calculation can be considered as a very simplified approximation to the silicon Auger lineshape in the first oxidation stages

since surface reconstruction or many-body effects (even treated at a self-consistent level) have not been included.

Acknowledgments

We are indebted to Dr H Pastawski and Dr R Koropecki for helpful discussions and for critically reading the manuscript. The Instituto de Desarrollo Technológico para la Industria Química belongs to the Consejo Nacional de Investigaciones Científicas y Técnicas (CONICET) and Universidad Nacional del Litoral. This work was performed under Grant PID 905607 from CONICET.

References

[1] Hollinger G, Bergignat E, Chermette H, Himpsel F, Lohez D, Lanoo M and Bensoussan M 1987 *Phil. Mag.* B **55** 735
[2] Hollinger G and Himpsel F 1983 *J. Vac. Sci. Technol.* A **1** 640
[3] Hollinger G, Morar J F, Himpsel F J, Hughes G and Jordan J L 1986 *Surf. Sci.* **168** 609
[4] Chen M, Batra I P and Brundle C R 1979 *J. Vac. Sci. Technol.* **16** 1216
[5] Schaefer J A and Göpel W 1985 *Surf. Sci.* **155** 535
[6] Garner C M, Lindau I, Su C Y, Pianetta P and Spicer W E 1979 *Phys. Rev.* B **19** 3944
[7] Carrière B, Deville J P and El Maachi A 1987 *Phil. Mag.* B **55** 721
[8] Morgen P and Onsgaard J 1980 *Surf. Sci.* **99** 87
[9] Muñoz M C, Martínez V, Tagle J A and Sacedón J L 1980 *J. Phys. C: Solid State Phys.* **13** 4247
[10] Vidal R, Koropecki R, Arce R and Ferrón J 1987 *J. Appl. Phys.* **62** 1054
[11] Ciraci S, Ellialtioğlu S and Erkoc S 1982 *Phys. Rev.* B **26** 5716
[12] Lander J J 1953 *Phys. Rev.* **91** 1382
[13] Feibelman P J and McGuire E J 1977 *Phys. Rev.* B **15** 2202
[14] Kunjunny T and Ferry D K 1981 *Phys. Rev.* B **24** 4604
[15] Kunjunny T and Ferry D K 1981 *Phys. Rev.* B **24** 4593
[16] Vidal R, Passeggi M C G, Goldberg E C and Ferrón J 1988 *Surf. Sci.* **201** 97
[17] Batra I P, Bagus P S and Hermann K 1984 *Phys. Rev. Lett.* **52** 384
[18] Lee Chongmu 1987 *Phys. Rev.* B **36** 2793
[19] Matthew J A D and Komninos Y 1975 *Surf. Sci.* **53** 716
[20] Ballhausen C J and Gray H B 1964 *Molecular Orbital Theory* (New York: Benjamin) p 229
[21] Bisi O and Calandra C 1981 *J. Phys. C: Solid State Phys.* **14** 5479
[22] Clementi E 1965 *IBM J. Res. Dev. Suppl.* **9** 2
[23] Clementi E and Raimondi D L 1963 *J. Chem. Phys.* **38** 2686
[24] Sferco S and Passeggi M C G 1985 *J. Phys. C: Solid State Phys.* **18** 3717
[25] Larkins F P 1971 *J. Phys. C: Solid State Phys.* **4** 3065
[26] Goldberg E C 1980 *Thesis* Universidad Nacional de Cuyo, Argentina
[27] Feibelman P J and McGuire E J 1978 *Phys. Rev.* B **17** 690
[28] Shirley D A 1972 *Phys. Rev.* B **5** 4709
[29] Jennison D R 1978 *Phys. Rev.* B **18** 6865
[30] Mulliken R S 1955 *J. Chem. Phys.* **23** 1833
[31] Ramaker D E, Hutson F L, Turner N H and Mei W N 1986 *Phys. Rev.* B **23** 2574